Available online at www.sciencedirect.com
SCIENCE DIRECT®
Journal of Colloid and Interface Science 267 (2003) 178–193
JOURNAL OF Colloid and Interface Science
www.elsevier.com/locate/jcis

Aggregation and solubility behavior of asphaltenes and their subfractions

P. Matthew Spiecker, Keith L. Gawrys, and Peter K. Kilpatrick *

Department of Chemical Engineering, North Carolina State University, Raleigh, NC 27695, USA

Received 13 December 2002; accepted 6 June 2003

Abstract

Asphaltenes from four different crude oils (Arab Heavy, B6, Canadon Seco, and Hondo) were fractionated in mixtures of heptane and toluene and analyzed chemically, by vapor pressure osmometry (VPO), and by small angle neutron scattering (SANS). Solubility profiles of the asphaltenes and their subfractions indicated strong cooperative asphaltene interactions of a particular subfraction that is polar and hydrogen bonding. This subfraction had lower H/C ratios and modestly higher N, V, Ni, and Fe contents than the less polar and more soluble subfraction of asphaltenes. VPO and SANS studies indicated that the less soluble subfractions formed aggregates that were considerably larger than the more soluble subfractions. In general, asphaltene aggregate size increased with decreasing solvent aromaticity up to the solubility limit, beyond which the aggregate size decreased with heptane addition. The presence of a low wavevector Q feature in the scattering curves at 25 °C indicated that the individual aggregates were flocculating; however, the intensity of the feature was diminished upon heating of the samples to 80 °C. The solubility mechanism for Canadon Seco asphaltenes, the largest aggregate formers, appears to be dominated by aromatic π-bonding interactions due to their low H/C ratio and low nitrogen content. B6 and Hondo asphaltenes formed similar-sized aggregates in heptol and the solubility mechanism is most likely driven by polar interactions due to their relatively high H/C ratios and high nitrogen contents. Arab Heavy, the least polar asphaltene, had a H/C ratio similar to Canadon Seco but formed the smallest aggregates in heptol. The enhancement in polar and π-bonding interactions for the less soluble subfraction indicated by elemental analysis is reflected by the aggregate size from SANS. The less soluble asphaltenes contribute the majority of species responsible for aggregation and likely cause many petroleum production problems such as pipeline deposition and water-in-oil emulsion stabilization.

1. Introduction

The study of asphaltene colloidal properties has been motivated by their propensity to aggregate, flocculate, precipitate, and adsorb onto interfaces. The tendency of asphaltenes to participate in colloidal and interfacial phenomena has posed great challenges for the petroleum industry. Problems associated with well production, pipeline transfer, land- and sea-based transportation, and ultimately oil refining have all been linked to the presence of asphaltenic colloids [1–13]. During visbreaking and catalytic hydrocracking large amounts of sludge and sediment can form [14], ostensibly due to the flocculation of asphaltenes during processing [15]. Coke generation and asphaltene adsorption within catalytic cracking beds can reduce the effective catalyst surface area as well as the efficiency of coal hydropyrolysis [16]. Asphaltene deposition within reservoir rocks has been blamed for pronounced reductions in well productivity [17]. Asphaltenes have also been found to facilitate the formation of extremely stable water-in-crude-oil emulsions [5,18–26]. Understanding asphaltene chemistry and the fundamental mechanisms of colloid formation has been the driving force behind much petroleum research for the past half-century.

Asphaltenes are defined as the portion of crude oil insoluble in n-alkanes such as n-heptane or n-pentane yet soluble in benzene or toluene [27,28]. The "solubility class" definition of asphaltenes generates a broad distribution of molecular structures that can vary greatly from one crude oil to another. In general, asphaltenes are characterized by fused ring aromaticity, small aliphatic side chains, and polar-heteroatom-containing functional groups. It is common to characterize asphaltenes by their average properties (see Table 1). The most common techniques for determining the chemical composition of asphaltenes include combustion el-

* Corresponding author.
E-mail address: peter-k@eos.ncsu.edu (P.K. Kilpatrick).

0021-9797/$ – see front matter
doi:10.1016/S0021-9797(03)00641-6

Table 1
Typical values of elemental compositions in asphaltenes

Element (wt%)	
H/C atomic	1.0–1.2
Nitrogen	1.0–1.2
Sulfur	2.0–6.0
Oxygen	0.8–2.0
Vanadium (ppm)	100–300

emental analysis (H/C, N, S) [29–33] inductively coupled plasma mass spectrometry (V, Ni, Fe) [34–38], and Fourier transform infrared spectroscopy (polar functional group concentrations) [39–44]. A wealth of information can be drawn from these chemical analyses. Atomic H/C ratios between 1.0 and 1.2 and N, S, and O content of a few weight percent suggest that much of the asphaltene backbone consists of fused aromatic carbons interspersed with polar functional groups containing five to seven heteroatoms per molecule. The specific orientation of polar and aromatic functional groups within the internal structure of asphaltene molecules is an ongoing subject of debate. FTIR analysis reveals many groups capable of forming hydrogen bonds, including carboxylic acids, carbonyls, phenols, and pyrrolic and pyridinic nitrogen [45–49]. These groups are capable of donating or accepting protons inter- and intramolecularly. The most plausible mechanisms of asphaltene aggregation involve π–π overlap between aromatic sheets, hydrogen bonding between functional groups, and other charge transfer interactions. The degree to which aggregate sizes vary is controlled by the polydispersity and chemistry of asphaltene monomers. While these chemical analyses provide valuable information concerning asphaltene chemistry and offer possible mechanisms of interaction, they do not directly probe the colloidal properties of asphaltenes.

The notion of asphaltenes forming colloidal aggregates in crude oil was originally proposed by Nellensteyn [1] and later by Pfeiffer and Saal [2]. They suggested that "dispersions" of asphaltenic aggregates in heavy crudes are solvated by resins and other aromatic compounds. X-ray diffraction measurements by Yen et al. suggested that asphaltene molecules contain a core or several cores of fused aromatic rings with an aliphatic periphery [28]. The flat aromatic core permits cofacial stacking of approximately four to five parallel sheets mediated by π–π bonding [4]. These early structural examinations were followed by more detailed and revealing investigations of the mechanisms of asphaltene aggregation and colloid formation [8,50–52].

The extent of asphaltene aggregation can be obtained from molar mass and neutron or X-ray scattering measurements. Asphaltene molecular weights have been probed by numerous techniques to yield values from one to several thousand daltons. The most common technique for measuring number average molecular weights is vapor pressure osmometry in an aromatic and/or polar solvent (e.g., toluene, benzene, pyridine, or *o*-dichlorobenzene) at elevated temperature (50–130 °C) [53–59]. Typical molar masses range from ca. 800 to 3000 g/mol in the best solvents. The dissociating power of each solvent varies and the smallest molar mass value observed is not necessarily indicative of the molar mass of an asphaltene monomer. Molar mass variations with solvent and temperature suggest changes in aggregate size rather than conformational changes in asphaltene structure. Interaggregate π-bonding and hydrogen bonding are far weaker than covalent bonding between carbon atoms and can be broken down in the presence of a good solvent at higher temperatures. MW values of 3000–6000 g/mol are typically obtained in toluene, suggesting that asphaltenes are associated under these solvent conditions into small oligomers of three to six monomers.

Small-angle neutron scattering (SANS) and small-angle X-ray scattering (SAXS) are powerful tools to deduce sizes and morphologies of colloidal aggregates in solution. Numerous studies have been performed over the past decade to probe the effects of solvent, temperature, and crude oil source on asphaltene aggregate size and polydispersity [8,11,13,51,52,60–74]. While both X-ray and neutron scattering can provide colloidal structure information, SANS offers the advantage of solvent–solute contrast via deuteration to decrease data collection times and probe the entire asphaltene aggregate. SAXS, on the other hand, can only discern the aromatic asphaltene core.

Proper analysis of the scattering intensity curves can provide aggregate size (R_g or ξ), shape, molecular weight, and fractal aggregate dimension. However, careful consideration of the molecular picture presented earlier can help guide the analysis. The most logical shape to consider might be a flat disk with a large diameter to thickness ratio. In addition, an asphaltene association model should consider asphaltene polydispersity. Mono- and polydisperse spheres [51,75], flat disks [12,60,62], prolate ellipsoids [64], and spherical vesicles [76], have all been suggested as possible asphaltene structures. Sheu et al. suggested that a polydisperse spheres model with a Schultz distribution best fit their scattering data [75]. Porte et al. suggested that asphaltenes aggregate through 2-D stacking interactions in which the highly flexible monomolecular sheets spontaneously bend out of the aromatic plane, forming hollow spherical vesicles [76]. This vesicle model was quantitatively consistent with both scattering and viscosity data. Lin et al. fit $Q > 0.01$ Å^{-1} data to a disk-like model with average R_g around 40 Å [69]. At smaller Q values (i.e., larger length scales), the data suggest the presence of larger aggregates or particles too sizeable to probe by Guinier analysis. They suggested that these large particles had diameters of approximately 1000 Å and often formed at high concentrations and/or low temperatures. Overfield et al. measured the R_g of vacuum resid asphaltenes in deuterated toluene at several temperatures [51]. R_g decreased from 116 Å at 25 °C to 55 Å at 100 °C and was explained by aggregate dissociation rather than an asphaltene conformational change. Aggregate size changes caused by temperature variation were, however, reversible. Espinat et al. measured the scattered intensity from asphaltenes in

several solvents and at low and high temperature [62]. In toluene, 2 wt% Boscan asphaltene solutions formed larger aggregates at room temperature (diameter 234 Å) than at 76 °C (175 Å). At room temperature, aggregate sizes were two to four times smaller in high-polarity solvents such as pyridine and tetrahydrofuran than in benzene. However, at elevated temperatures (up to 80 °C), the solvent effect was less significant and aggregate size approached a minimum. Increased heptane fraction in mixtures of heptane and toluene tends to enhance asphaltene aggregation and lead to higher R_g values [13]. Fenistein and Barré fractionated asphaltenes by ultracentrifugation and found that R_g and molecular weight increased with fraction density/weight [72]. Roux et al. used SANS to study temperature and concentration effects on the structure of Safaniya asphaltenes in toluene [74]. At asphaltene volume fractions less than 3–4%, aggregates were well solvated with molecular weights on the order of 10^5 g/mol and R_g values from 30 to 90 Å.

Molecular weights determined from neutron scattering of polydisperse asphaltene systems are weight-averaged and may be biased by the presence of a small number of high-mass aggregates. As the aforementioned aggregate size data suggest, asphaltene solubility can vary appreciably in solvents containing different polarities and aromatic carbon content. Solvents that more closely resemble and interact with asphaltene microstructure can effect a greater state of dissolution than low polarity, aliphatic solvents. The application of heat can further disrupt the aggregation process and reduce the equilibrium aggregate size. Through asphaltene solubility and aggregate size measurements in different solvents and temperature regimes, we will begin to unravel the complex mechanisms of aggregation. By fractionating and concentrating the more polar and aromatic material, we should be able to enhance the degree of asphaltenic aggregation. Several recent studies have probed the effects of asphaltene fractionation by differential solubility in terms of chemical composition. Nalwaya et al. [35] and Kaminski et al. [77] have fractionated asphaltenes in mixtures of pentane and methylene chloride to analyze their chemistry and dissolution kinetics. Higher polarity fractions had lower rates of dissolution compared to lower polarity fractions. These authors linked the high polarity to heteroatom and metal content, particularly iron, nickel, and vanadium.

Yarranton and Masliyah employed solubility and precipitation methods to study the solution behavior of heptane-precipitated Athabasca asphaltenes [58]. Asphaltenes were added to premixed hexane–toluene solutions and then filtered in the solubility method. The precipitation method involved complete dissolution in toluene followed by hexane addition and filtration. Both methods yielded identical mass fractions of insoluble asphaltenes except at low solute concentrations. At a toluene volume fraction equal to 0.5, less than 10% (w/w) of the asphaltenes were insoluble. Presumably, the insolubles mass fraction was negligible in solvents that were more aromatic. Of greater significance, molar masses were inversely proportional to the extent of precipitation. For example, the sub-fraction comprising roughly 35% of the least soluble asphaltenic material had a VPO molar mass value in toluene at 50 °C of approximately 7000 g/mol while the unfractionated asphaltenes had a molar mass of approximately 3000 g/mol. As the solvent blends became less aromatic, the fraction precipitated increased and molar mass decreased. These results suggest that the asphaltenes most prone to precipitation form the largest aggregates in solution.

Andersen et al. studied the precipitation of asphaltenes in mixtures of heptane and toluene from undiluted Boscan crude oil and from the heptane insoluble portion of Boscan crude [57]. They found that asphaltenes were more soluble in crude oil (presumably due to resins and other aromatics) than in heptane–toluene blends that mimicked the crude composition. Enhanced solubility reduced the yield of insolubles and concentrated the more polar and aromatic structures as evidenced from fluorescence measurements. Of greatest consequence was the large difference between soluble and insoluble asphaltene molar masses by VPO. The soluble asphaltenes formed aggregates nearly five times smaller than corresponding insoluble asphaltenes.

In this work, we have determined the solubility profiles of four asphaltenes in mixtures of heptane and toluene, or so-called "heptol" mixtures, at fixed concentration. At solvent conditions where asphaltenes precipitate (high ratios of heptane to toluene), we have isolated the soluble and insoluble material for further study. Additional solubility profiles were prepared for the more and less soluble fractions in heptol. Detailed chemical analyses were performed to measure the degree of polarity and aromaticity in the insoluble fraction. Intermolecular interactions were probed with SANS in various heptol mixtures at 25 and 80 °C. Comparison of asphaltene fraction chemical composition to solubility and aggregate size data can help elucidate the mechanism of asphaltene aggregation and its dependence on chemistry and solvency. Heuristics and fundamental understanding, gleaned from careful scattering and nanostructural studies, can make it possible to mitigate the deleterious effects of asphaltene aggregation, precipitation, and deposition.

2. Experimental

2.1. Asphaltene source

Asphaltenes were precipitated from four crude oils: B6 and Hondo (off-shore California), Arab Heavy (Safaniya), and Canadon Seco (Argentina). For brevity the following abbreviations will be used to describe the asphaltenes generated from Hondo, Arab Heavy, and Canadon Seco crude oils, respectively: HO, AH, and CS. These crude oils are asphaltene-rich and vary in viscosity, resin-to-asphaltene (R/A) ratio, and asphaltene H/C ratio and heteroatom content. Basic crude oil and asphaltene properties are summarized in Table 2.

Table 2
Crude oil properties

Crude	Wt% asph	R/A ratio (w/w)	H/C asph atomic	Viscosity (cP) 100 °F
AH	6.7	1.12	1.14	33.8
B6	13.1	0.92	1.22	2030
CS	7.5	1.19	1.11	70
HO	14.8	1.39	1.29	363

2.2. Asphaltene precipitation

All crude oils were stored near 0 °C in sealed containers under an argon blanket to minimize possible oxidation. The crude oil was warmed to room temperature and shaken vigorously to ensure homogeneity before sampling. Several (typically 6–8) aliquots of 15–20 g of crude oil were diluted with *n*-heptane 40:1 by volume and gently shaken for 24 h. Since the crude oils were viscous and only partially soluble in heptane, the flasks were initially hand shaken to completely disperse all material. After the continuous shaking, the precipitated asphaltenes were removed by vacuum filtration through 15-cm-diameter 1.5-µm Whatman 934-AH glass microfiber filter paper. The filter cake was rinsed with 10-ml aliquots of *n*-heptane to remove any maltenes that may have reported to the "soluble" fraction. All solvents used were HLPC grade and obtained from Fisher Scientific. Additional aliquots of heptane were added to the filter cake until the washings eluted through the filter paper were clear in color. The filtrate was isolated and methylene chloride was used to redissolve the asphaltenes under partial vacuum. The methylene chloride–asphaltene solution was rotary evaporated under partial vacuum at 40 °C. After evaporating a substantial volume of solvent, the remaining solution was transferred to glass jars and placed under an argon stream for further drying. Once nearly dry, the samples were moved into a nitrogen-flushed vacuum oven at 50 °C for 24–36 h. Throughout the remainder of this paper, the asphaltenes isolated from the original crude source will be referred to as the "Whole" asphaltenes.

2.3. Asphaltene solubility determination

The solubility of all asphaltenes was determined gravimetrically in mixtures of heptane and toluene. Asphaltene solutions with a concentration of 0.75% (mass solute/volume solvent) or ∼1 wt% were prepared by dissolving the asphaltenes (∼0.1125 g) in 15 ml of a heptol. Asphaltenes were completely dissolved in toluene prior to the addition of heptane, which served as a nonsolvent, and the solutions were allowed to equilibrate for 12 h. The solutions were then vacuum filtered through 5.5-cm-diameter 1.5-µm Whatman 934-AH glass microfiber filter paper and a rinse solvent (7.5 ml) of equivalent heptol composition was poured immediately onto the filter cake to remove any remaining soluble material. The filtrate was isolated and the precipitate was redissolved using warm methylene chloride. Two solutions were generated during the fractionation process: one solution containing the more soluble or so-called "Soluble" asphaltenes in heptol and the other containing the less soluble or so-called "Precipitate" asphaltenes in methylene chloride. Each solution was rotary evaporated and dried in a nitrogen-flushed 50 °C vacuum oven for 24 h. The solubility of asphaltenes in heptol was subsequently gauged by the mass percentage of material that precipitated in a particular solvent mixture. A solubility profile for the "Whole" asphaltene was generated by performing the above gravimetric experiments under a range of solvent compositions. To probe the chemical differences between the asphaltenes that precipitated and those that remained soluble, each asphaltene was separated into Precipitate and Soluble fractions at the preparative scale. The corresponding heptol mixture needed to generate the Precipitate and Soluble fractions was asphaltene-specific and was chosen to generate an approximate 1:2 mass ratio of Precipitate to Soluble. The Precipitate and Soluble fractions had markedly different chemical compositions and physical properties and sufficient material was generated per batch for the subsequent analyses.

2.4. Chemical characterization

Elemental analysis (C, H, N, S, and O) and vapor pressure osmometry were performed by Darlene Mahlow at the University of Alberta (Department of Chemistry, Edmonton, Alberta, Canada). Number-average molecular weights of selected asphaltenes were determined in toluene at 53 °C with a Corona Wescan vapor pressure osmometer. In the VPO device, vapor pressure is measured indirectly using two thermistors to measure voltage changes (ΔV) caused by changes in temperature. The measuring chamber contains a solvent reservoir and two wicks that provide a saturated solvent atmosphere around the thermistors. At one thermistor, the pure solvent is replaced by solution. Subsequent condensation of the solvent from the saturated atmosphere into solution releases heat and increases the thermistor temperature. Condensation and thermistor temperature will increase until the vapor pressure of the solution matches that of the pure solvent at the given chamber temperature. Solutions were prepared at concentrations ranging from 1 to 20 mg/ml. The values of $\Delta V/C$ at each concentration were converted to an apparent molar mass using the calibration factor determined for a standard solute (Benzil). Metal analyses (Fe, Ni, V, and Na) were performed at Ondeo-Nalco Energy Systems (Sugar Land, TX). Metals content was determined by the inductively coupled plasma (ICP) method with a Jerrel Ash 9000 after the samples were ashed at 600 °C and dissolved in HCl and deionized water.

2.5. Small angle neutron scattering: 25 °C

Neutron scattering is an important technique for determining solute aggregate sizes on a submicrometer scale. A broad wave vector (Q) range, high neutron flux, and large

number of scatterers are the ideal conditions to probe the scattering behavior of aggregates. Most of the SANS measurements reported were performed on the 30-m NG7 and 8-m NG1 small-angle spectrometers at the National Institute of Standards and Technology Center for Neutron Research (Gaithersburg, MD), with the exception of the SANS data presented in Fig. 9, which were collected on the small-angle neutron diffractometer (SAND) instrument at the Intense Pulsed Neutron Source at Argonne National Laboratory (Argonne, IL).

During the SANS (NIST) experiments, the source-to-sample distance was varied from 4 to 16 m while the sample-to-detector distance was varied from 1.2 to 15 m. Neutrons of 6-Å and 0.22 spread ($\Delta\lambda/\lambda$) were scattered from the sample and collected on a two-dimensional detector (65 cm by 65 cm, 1 cm by 1 cm resolution). The instrument geometry and neutron wavelength values bound the operating Q range following the equation

$$Q = 4\pi\lambda^{-1}\sin\theta, \tag{1}$$

where θ is half of the scattering angle and λ is the neutron wavelength. The available Q range extended from 0.0015 to 0.6 Å^{-1} but an intermediate range of 0.0022 to 0.3 Å^{-1} was adequate for most asphaltene solutions.

Asphaltene solutions of 1% (w/w) were prepared in perdeuterated solvents—toluene and heptane or 1-methylnaphthalene—to enhance scattering contrast. Solvents were obtained from CDN Isotopes and had >99.9% chemical purity and >99.5% perdeuteration. Dissolution was performed first in perdeuterated toluene followed by heptane addition and equilibration over several days. All solutions were transferred from the glass vials to the quartz cells without filtration, even in the cases where some precipitation was evident.

Samples were measured at 25 °C in cylindrical quartz sample cells (NSG Precision Cells) with a path length of 5 mm. During beam operation, samples were run at high Q with the detector positioned 1.2 m from the sample (large θ). The scattering intensity, $I(Q)$, was obtained from the total detector counts corrected for neutron transmission through the sample, background radiation, scattering through an empty cell, and detector sensitivity. For the data collected, it was necessary to splice the low-Q and high-Q data obtained from different detector positions.

The small angle neutron diffractometer (SAND) instrument at Argonne National Laboratory is a time-of-flight diffractometer attached to an accelerator-based pulsed neutron source (30 Hz). Each pulse contained neutrons with wavelengths ranging from 1 to 14 Å. The higher energy neutrons had lower wavelengths and reached the sample ahead of the lower energy neutrons. Thus, the energy of each scattered neutron was determined by its time of flight to the detector. The sample-to-detector distance was fixed at 2 m. Neutrons were collected on an area detector (40 cm by 40 cm, 4 to 6 mm FWHM resolution). The available Q range extended from 0.0035 to 2 Å^{-1}. The data presented in Fig. 9 were collected at 25 °C in cylindrical quartz sample cells (NSG Precision Cells) with a path length of 2 mm.

2.6. Small angle neutron scattering: 80 °C

High-temperature neutron scattering of the asphaltene samples was performed on both NG1 (8-m) and NG7 (30-m) beamlines. Both instruments had multisample holders, with attached circulating water–glycol baths, capable of maintaining 80 °C. All samples were initially dissolved in toluene and underwent a temperature cycle (80 °C, 1 h) prior to heptane addition to ensure complete dissolution. Immediately prior to measurement, the asphaltene solutions were transferred to 5-mm path length quartz cells and placed in an 80 °C bath for 1 h. This time allowed the solutions to reach thermodynamic equilibrium.

3. Data handling

Scattering intensity versus scattering angle ($I(Q)$ vs Q) curves were fit to Lorentzian lineshapes using nonlinear least-squares regression to determine the aggregate size and morphology. Following the Ornstein–Zernike formalism the scattering intensity, I, can be related to the scattering vector, Q, by

$$I(Q) = \frac{I_0}{1 + (Q\xi)^2}, \tag{2}$$

where I_0 is the zero-Q scattering intensity and ξ is the correlation length [71,78]. In some systems, a Porod upturn was observed at low Q where the scattering intensity increased monotonically with decreasing Q. Roux et al. observed a similar low-Q feature for Safaniya asphaltenes in toluene, particularly at low temperature (i.e., 8 and 20 °C), that diminished in intensity with heating [74]. A low-Q upturn indicates the presence of large flocs of primary aggregates in solution. Incoherent scattering of all nuclei in the solvent and solute with nonzero spin was also manifested in the scattering curves at large Q values (typically $Q > 0.1$) as an isotropic background signal. The Q values that marked the transition between the various length scales of aggregation were determined from inflection points in the scattering curves. The Lorentzian lineshape described in Eq. (2) was applied to all samples over the intermediate range of Q values between the inflection points.

The zero-Q scattering intensity, I_0, provides additional information concerning the particle geometry and is related to the weight-average molecular weight (M) of the aggregates by the expression

$$I_0 = \frac{\Delta\rho^2 C M}{N_A d^2}, \tag{3}$$

where N_A is Avogadro's number, C is the concentration of scatterers in g/ml, d is the scatterer density, and $\Delta\rho^2$ is the coherent scattering contrast between the solvent and

solute. Given that elemental compositions of the asphaltenes are available, it is possible to calculate the scattering contrast terms, and subsequently, the weight-average molecular weight of the aggregates; however, this calculation and subsequent comparison to asphaltene aggregate sizes will be addressed in a future paper.

4. Results and discussion

Solubility profiles for the Whole asphaltenes isolated from AH, B6, CS, and HO crude oils were determined by the previously described gravimetric method (Fig. 1). The asphaltenes were completely soluble in pure toluene and in heptol mixtures of high aromaticity (>52% (v/v) toluene). The observed amount of precipitated material increased with heptane addition in the insoluble regime. The critical heptol concentration for the initial formation of precipitates ranged from 45–52% (v/v) toluene depending on the asphaltene. The addition of heptane to toluene reduced the dispersive and polar components of the solubility parameters of the solvent [79,80], resulting in flocculation and precipitation of the asphaltene aggregates.

Andersen et al. [57] performed a series of precipitation and redissolution experiments on Boscan asphaltenes in heptol. The direct addition of heptol to the crude oil precipitated less material than observed in Fig. 1, likely due to the solubilizing effects of resins and other aromatic components present in the crude oil; however, the results obtained for redissolution of precipitated asphaltenes agreed closely with those shown in Fig. 1. For example, Andersen observed that 13, 46, and 60% (w/w) of the asphaltenes precipitated in solvent compositions of 50, 40, and 30% (v/v) toluene, respectively. The Boscan asphaltenes were slightly less soluble than CS, the least soluble asphaltene presented in Fig. 1.

The process of precipitation was likely controlled by dispersion and π–π bonding interactions between the asphaltenes and the solvent mixture, as suggested by the refractive index measurements performed by Buckley [81,82].

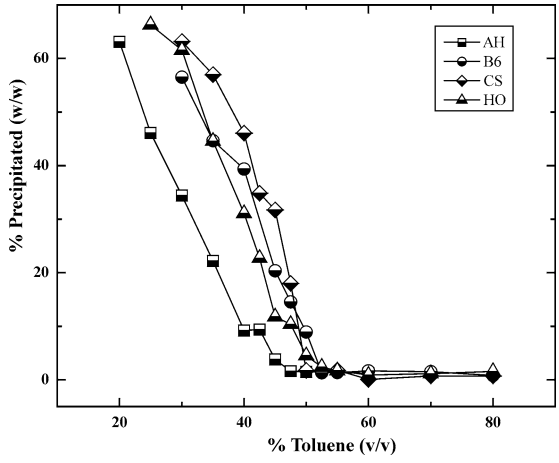

Fig. 1. Solubility profiles of Whole asphaltenes in heptol.

Buckley performed heptane titration experiments on an Alaskan crude oil dissolved in toluene and various solvents and observed a nearly constant value of the index of refraction for the solution at the solubility limit [81]. Buckley also showed that asphaltene precipitation was reversible by adding toluene to a precipitated mixture of crude oil in heptane and observing that the asphaltenes completely redissolved in solutions with the same refractive index value at which they initially precipitated [82]. Porte et al. proposed that while precipitation was controlled by weak dispersion forces, asphaltene aggregation was driven by strong specific polar and hydrogen-bonding forces [76]. As previously mentioned, asphaltenes are characterized by their high aromaticity, the presence of polar heteroatoms, and their ability to participate in hydrogen-bonding interactions. If asphaltenes containing a higher percentage of fused aromatic rings and polar heteroatoms tend to form the largest aggregates in solution, then it seems reasonable that these species would be the first to precipitate from solution as the solvent quality decreases below the solubility limit.

4.1. Asphaltene fractionation

To test the hypothesis that fractionation concentrated the more aromatic and polar asphaltenes in the less soluble fractions, so-called “Soluble” and “Precipitate” fractions were prepared for the various asphaltenes on a preparatory scale. The fractionation conditions and amounts of each fraction generated are shown in Table 3. Due to its high solubility, AH was precipitated at the highest ratio of heptane to toluene. The other three asphaltenes underwent fractionation at heptol ratios close or equal to 40% toluene. Throughout the course of the study, AH and B6 were fractionated three times each, with reasonable reproducibility (see Table 3).

There were several differences observed between the Precipitate and Whole asphaltenes. After the initial filtration and heptol rinse steps, the Precipitate fraction remaining on the filter paper was significantly less soluble in methylene chloride than the Whole asphaltenes. The less soluble fractions

Table 3
Asphaltene fractionation results (wt%)

Asphaltene	*n*-Heptane–toluene ratio	Precipitate	Soluble
AH	70:30	38.4	61.6
		34.4	65.6
		32.2	67.8
Average		35±3	65±3
B6	60:40	33.2	66.8
		31.6	68.4
		32.4	67.6
Average		32.4±0.8	67.6±0.8
CS	60:40	35.7	64.3
HO	61:39	28.2	71.8
		33.1	66.9
Average		30.7	69.3

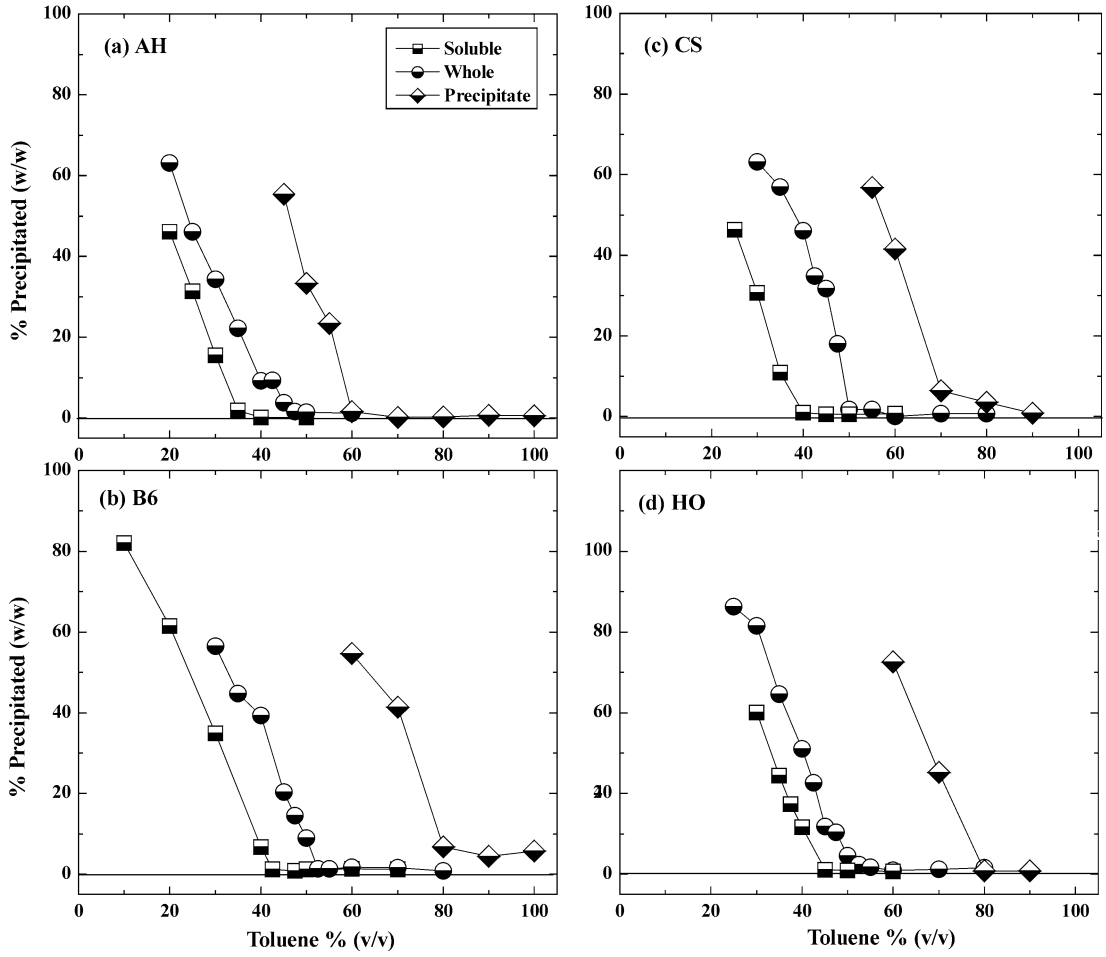

Fig. 2. Solubility profiles of Whole, Soluble, and Precipitate asphaltenes in heptol.

of B6, CS, and HO required submergence in warm to hot solvent for several minutes to completely redissolve. This behavior indicates the Precipitate fraction had an enhanced degree of interaggregate bonding compared to the Whole and Soluble fractions. The Soluble fraction appears to cooperatively solvate the Precipitate fraction through disruption of the strong polar and hydrogen-bonding interactions that drive self-association in the Precipitate fraction.

Solubility curves of the Soluble and Precipitate asphaltenes are shown in Figs. 2a–2d. The Precipitate solubility curves provided the most convincing support for selective cooperative solvation as an important component enhancing asphaltene solubility. For example, one would expect that if the B6 Precipitate asphaltenes were non-interacting, these molecules would begin to precipitate at the same heptol ratio as B6 Whole (∼52% toluene) and become completely insoluble at the original fractionation condition of 40% toluene. However, removal of the Soluble fraction from the Whole asphaltenes caused the Precipitate fraction to become insoluble at a higher toluene volume fraction than expected, particularly with B6 and HO. In fact, the B6 Precipitate fraction was observed to be slightly insoluble in pure toluene.

Also noteworthy was the solubility behavior of the Soluble asphaltenes at the same heptol ratios used for their preparation. One would expect AH Soluble to be completely soluble in 30% toluene; however, ∼15% of the asphaltenes precipitated at this condition. Both B6 and HO Soluble demonstrated this “early” precipitation behavior to a lesser degree, while CS Soluble behaved “ideally.” In these cases, it is likely that the Solubles may benefit from some portion of the Precipitate to help them retain solubility. In all cases, the Soluble fraction was far more soluble than either the Whole or Precipitate fractions. Removing the Soluble fraction from the Precipitate fraction dramatically decreased the kinetics of dissolution and the ultimate solubility of the Precipitate fraction. In this sense, the Soluble fraction acted cooperatively to keep the more aromatic and polar material in solution.

Strictly speaking, solubility profiles for the Soluble and Precipitate fractions would have been best compared to the Whole asphaltenes when dissolved at heptol concentrations that mimicked the fractionation condition—0.25% (w/v) for the Precipitate fraction and 0.5% (w/v) for the Soluble fraction. However, solubility studies by Cimino et al. [17]

and Porte et al. [76] indicated that the onset of precipitation is nearly independent of dilution at low concentrations (<2 wt%). Cimino et al. dissolved pentane precipitated asphaltenes from a light crude oil in several different solvents at ambient conditions and titrated with an anti-solvent until the precipitation threshold was observed [17]. The authors plotted the mass ratio nonsolvent:asphaltene vs the mass ratio solvent:asphaltene and observed a linear dependence of the two variables, suggesting that asphaltene concentration did not affect the solubility limit over the range of concentrations studied. Porte et al. obtained similar results for Lagrave crude oil dissolved in toluene (solvent) and pentane (nonsolvent) [76]. The solubility limit corresponded to a pentane volume fraction of 0.5, regardless of concentration. The authors explained this observation by a small value of the entropy of mixing of the aggregates in the solvent. It seems reasonable to extend this assumption to the Whole, Soluble, and Precipitate fractions in this study, which only vary in terms of aromaticity and heteroatom content.

4.1.1. Asphaltene fraction chemistry

Combustion elemental analysis was performed to determine H/C ratio and polar heteroatom content in each fraction generated (i.e., Whole, Soluble, and Precipitate), as shown in Table 4. H/C ratio correlates well with aromaticity (i.e., a lower H/C ratio implies a greater number of fused aromatic rings). In all cases, the Precipitate fraction was enriched in aromatic carbon while the Soluble aromaticity was diminished. As shown in the table, nitrogen content decreased modestly with increasing asphaltene solubility. Nitrogen can be found in several functional forms including amines, amides (carbonyl amides), pyrroles, and pyridines. Some nitrogen-containing functional groups, such as pyridine, are basic and can participate in strong hydrogen-bonding interactions that are much greater than dispersion forces between aromatic asphaltenic cores. Sulfur is typically found in thiophenic rings, sulfides, and, to a smaller extent, in sulfoxide groups. Sulfoxides may be present because of asphaltene oxidation during handling. As stated previously, asphaltenes were handled under argon atmosphere to minimize oxidation. AH, B6, and HO asphaltenes contained much higher concentrations of sulfur than CS asphaltenes; however, there did not appear to be a correlation between asphaltene fraction or solubility behavior and sulfur content. Again, the variations from Soluble to Precipitate were subtle, but the increased polarity and aromaticity contributed significantly to the macroscopic solubility behavior.

This phenomenon was first observed by Szewczyk et al., who fractionated C_7 asphaltenes obtained from Rospomare crude oil in mixtures of σ-xylene and n-heptane [83]. Four complementary fractions of "Soluble" and "Insoluble" asphaltenes were isolated, with the Insoluble fractions (FI1 to FI4) consisting of 37, 56, 64, and 74% (w/w) of the unfractionated asphaltenes, respectively. Combustion chemical analyses showed that the Insoluble fractions were typically higher in aromaticity and heteroatom content (i.e., N and O) than the corresponding Soluble fractions. For the most part, sulfur content remained evenly distributed throughout the fractions. Chemical analysis of pyrolysis products suggested that oxygen was located near the periphery of the aggregates, causing them to be more accessible to aggregation through polar and hydrogen-bonding interactions. Many of the above observations (e.g., increase in nitrogen content and aromaticity with decreasing asphaltene yield and even distribution of sulfur species) were also verified by Andersen et al. in the chemical analyses of Boscan asphaltene fractions [57].

The results of metal analyses for the various asphaltene fractions are shown in Table 5. Ni and V are often bound within porphyrin rings in asphaltenes and have been associated with difficulties during hydrocatalytic upgrading of crude oils [84]. In general, the Precipitate fractions were enriched with Fe, Ni, V, and Na. B6 and HO fractions contained significantly more Ni and V than the AH and CS fractions. Kaminski et al. fractionated asphaltenes in mix-

Table 4
Asphaltene fraction composition in wt%, except H/C ratio (atomic)

Asphaltene	H/C			Nitrogen			Sulfur			Oxygen		
	Soluble	Whole	Precipitate	Soluble	Whole	Precipitate	Soluble	Whole	Precipitate	Soluble	Whole	Precipitate
AH	1.17	1.14	1.13	0.92	1.02	1.08	8.06	8.32	7.66	1.92	1.64	2.52
B6	1.30	1.24	1.22	1.81	1.87	1.93	7.25	6.68	6.33	2.67	2.9	2.81
CS	1.12	1.11	1.09	1.32	1.32	1.39	0.52	0.52	0.48	2.11	1.73	2.27
HO	1.30	1.29	1.24	1.95	1.99	2.11	8.42	8.53	8.48	2.51	2.1	2.66

Table 5
Metals analysis (ppm)

Asphaltene	Iron			Nickel			Vanadium			Sodium		
	Sol	W	Ppt	Sol	W	Ppt	Sol	W	Ppt	Sol	W	Ppt
AH	14	26	50	84	160	160	350	490	540	31	31	31
B6	7.9	35	47	350	330	410	1000	1000	1200	27	9300	25,000
CS	51	77	150	19	21	28	42	48	48	43	130	180
HO	6.3	16	12	340	360	410	930	950	1100	11.9	550	1800

tures of methylene chloride and pentane and found that the most polar fraction contained the highest concentrations of Fe, Ni, and V and typically had the lowest dissolution rates in dodecyl benzenesulfonic acid–heptane mixtures [77].

The relatively high concentration of Na in the B6 fractions may be due in part to its offshore source (see Table 5). Water containing dissolved salts may have been dispersed in the crude oil during the asphaltene precipitation and subsequently partitioned into the Precipitate fraction during the fractionation process. In order to test for the presence of water-soluble salts, B6 crude oil was dissolved in methylene chloride and extracted with deionized water in a separatory funnel. The Na content of the Whole asphaltenes precipitated from the water-extracted crude oil was reduced from 9300 to 35 ppm. Total Ca and K content was also reduced, while Ni, V, and Fe content remained unchanged. This suggests that the high alkali and alkaline earth metal content in B6 was attributable to either water-soluble inorganic salts or water-soluble soaps of corresponding carboxylic acids.

Based on the relative aromaticity and nitrogen content of the four Whole asphaltenes, some plausible explanations of precipitation can be offered. AH and CS Whole contained less nitrogen and had a relatively low H/C ratio compared to B6 and HO Whole asphaltenes. The aggregation mechanism for AH and CS asphaltenes was likely dominated by dispersion forces or differences between asphaltene and solvent aromaticity (π–π bonding interactions). B6 and HO Whole asphaltenes had relatively low aromaticities but were relatively nitrogen rich, suggesting that polar and hydrogen-bonding interactions may play a significant role in the asphaltene association mechanism. As we will demonstrate in the next section, variations in the chemical composition of the asphaltene fractions are linked to the size of aggregates formed in solution. In a subsequent paper, we will demonstrate the impact of aggregate formation on the stability of asphaltene-stabilized water-in-oil emulsions [85].

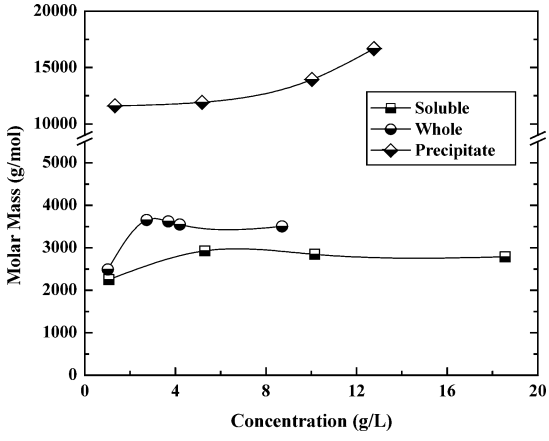

Fig. 3. VPO molar masses of B6 asphaltenes (Soluble, Whole and Precipitate) in toluene at 53 °C.

4.1.2. Vapor pressure osmometry of asphaltenes and their fractions

VPO apparent molar masses of B6 Soluble, Whole, and Precipitate fractions in toluene are shown in Fig. 3. B6 Soluble had the lowest molar mass of all the fractions, with a maximum value of ∼3000 g/mol. The limited number of data points does not allow accurate prediction of the zero-concentration molar mass; however, extrapolation of the two lowest concentration data points predicts a value of ∼2000 g/mol. B6 Whole was slightly more aromatic, polar, and less soluble than the Soluble fraction, and the molar mass values for B6 Whole were roughly 500 g/mol higher than the Soluble fraction over the concentration range studied. B6 Precipitate molar mass values were higher than the Whole and Soluble asphaltenes by almost an order of magnitude. Even at high dilution, the apparent molar mass of B6 Precipitate asphaltenes exceeded 10,000 g/mol, suggesting strong intermolecular interactions within the aggregate. B6 Precipitate asphaltenes were also more difficult to dissolve than the Whole and Soluble fractions. Nevertheless, the molar mass values observed for B6 Whole, Soluble, and Precipitate fractions were consistent with those obtained by Yarranton et al. [59]. For example, Yarranton et al. found that the molar mass values of heptane precipitated Athabasca asphaltenes increased with bulk concentration from ∼2000 g/mol at low concentration to a limiting value of ∼10,000 g/mol at 20 g/l (∼2 wt%). Low concentration extrapolation revealed apparent monomer molar masses of approximately 1000–2000 g/mol.

In contrast to B6 asphaltenes, CS Whole and Precipitate fractions had nearly identical molar masses at each concentration examined (Fig. 4). Extrapolation to zero concentration indicated minimum sized aggregate molar masses of approximately 3000 g/mol. The relatively low molar mass of CS Precipitate asphaltenes compared to B6 Precipitate suggests that heating of the samples to 53 °C might significantly disrupt the dispersion and π–π bonding forces that dominate asphaltene aggregation in CS asphaltenes, but is ineffective at disrupting the polar and hydrogen-bonding forces that dominate aggregation in B6 Precipitate asphaltenes. A simi-

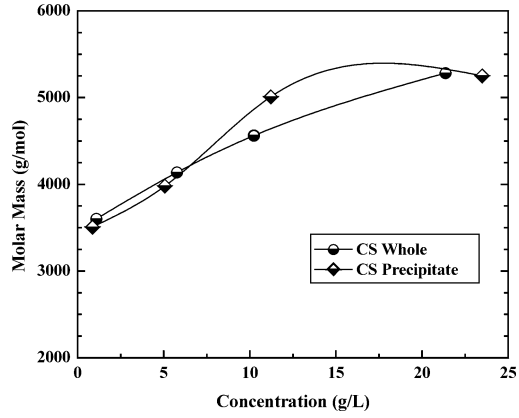

Fig. 4. VPO molar masses of CS (Whole and Precipitate) asphaltenes in toluene at 53 °C.

lar response to heating was observed for the fractions when studied by SANS at 25 and 80 °C, as seen in the next sections.

The VPO results presented in Figs. 3 and 4 show definite qualitative differences in the aggregation behavior of B6 and CS asphaltene fractions; however, the effect of precipitated solids within the samples on VPO measurements are not easily quantified. For example, the occurrence of 25,000 ppm of sodium in the B6 Precipitate fraction suggested that this fraction may have contained as much as 6% (w/w) inorganic solids, assuming that sodium occurred in the form of NaCl. The presence of NaCl in the fraction is not expected to interact appreciably with the solvent and affect the vapor pressure; however, uncertainty is introduced in the effective asphaltene concentration. Inorganic solids may have been present in other asphaltene fractions and affected the VPO measurements to a lesser extent (e.g., B6 Whole contained 9300 ppm sodium). Furthermore, voltage measurements collected at low concentrations (<1 g/l) were subject to greater uncertainty than those collected at higher concentrations due to low instrument sensitivity. The total uncertainty in any of the molar masses presented was estimated to be less than 20%. Within this estimated uncertainty, general qualitative differences in molar mass between the Whole, Soluble, and Precipitate fractions are readily apparent. The SANS measurements discussed in the next section will provide a more sensitive measurement of how asphaltene aggregate size varies within the fractions as a function of temperature and solvent conditions.

4.2. Small angle neutron scattering: 25 °C

Neutron scattering curves of intensity (I) versus scattering vector (Q) of B6 Whole asphaltenes in several mixtures of deuterated heptol are shown in Fig. 5. Based on the shape of the neutron scattering curve alone, one can readily distinguish solutions of small aggregates from flocculated systems. For example, the low-Q plateau behavior for B6 Whole asphaltenes in pure toluene indicated that the solution contained soluble, non-flocculating nanoparticle aggregates. The remaining B6 Whole scattering curves exhibited an intense low-Q feature superimposed on a Guinier plateau. The presence of a low-Q feature indicated that reduced solvent aromaticity was driving a small fraction of the nanoparticle aggregates to flocculate into microscale aggregates or "flocs" that retained their solubility in solution. The absence of a second plateau region in the lowest Q range suggested that the largest flocs had a size greater than the order of $1/Q_{\min}$ (or $\geqslant$1000 Å). The floc size must have been smaller than 1.5 μm, however, because all solutions above 55% toluene were soluble to filtration. As shown in the next section, the intensity of the low-Q upturn was observed to diminish with heating to 80 °C; however, a feature of similar scattering intensity reappeared with subsequent cooling of the sample to 25 °C, suggesting an equilibrium condition between the nanoparticle aggregates and microscale aggregates at this temperature. The relative ordering of the intensities at intermediate Q from Fig. 5 suggests that the nanoparticle aggregates were the largest in 55% toluene with aggregate size decreasing as the solvent quality became more aromatic.

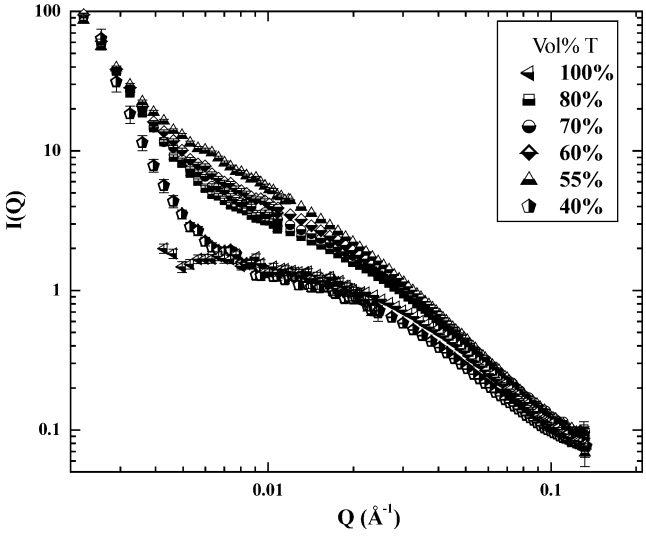

Fig. 5. SANS curves of B6 Whole asphaltenes in mixtures of d-heptane and d-toluene at 1 wt%, 25 °C.

Prior to measurement, partial precipitation was observed in the B6 Whole sample dispersed in 40% toluene. For this sample, the scattering intensity in the intermediate-Q range decreased relative to 55% toluene, suggesting that solvent conditions have driven the largest aggregates to precipitate, thus leaving the smaller, soluble aggregates behind in solution. In fact, the remaining soluble aggregates were half the size of those in 55% toluene, as shown in the following section. It can also be deduced from the figure that the size of the large agglomerates (i.e., precipitated material) in the 40% toluene sample was likely greater than those observed for the remaining soluble samples, as indicated by the steeper power law slope in the low-Q regime.

$I(Q)$ versus Q scattering curves were fit using the Ornstein–Zernike formalism to determine solute correlation lengths. Two examples of the Lorentzian fits are shown in Fig. 6. AH Soluble asphaltenes are well dissolved in 50% toluene (Fig. 6a) as shown by the Guinier plateau at low Q values ($\xi = 29.9$ Å). An example of an asphaltene exhibiting significant low-Q scattering is shown in Fig. 6b. In fitting scattering curves with this low-Q feature to Eq. (2), the low-Q upturn is truncated at the inflection point and the intermediate-Q portion of the scattering curve for B6 Whole in 60% toluene was fit to obtain a correlation length of 79 Å. In both cases, the data were truncated in the high-Q range to remove the effects of incoherent background scattering.

Correlation lengths deduced from SANS scattering curves of the Whole asphaltenes dissolved in solutions of varying heptol ratio appear in Fig. 7. For each of the asphaltenes the correlation length increased with decreasing toluene content within the soluble regime. This increase suggested that interaggregate associations increased as the solvating power

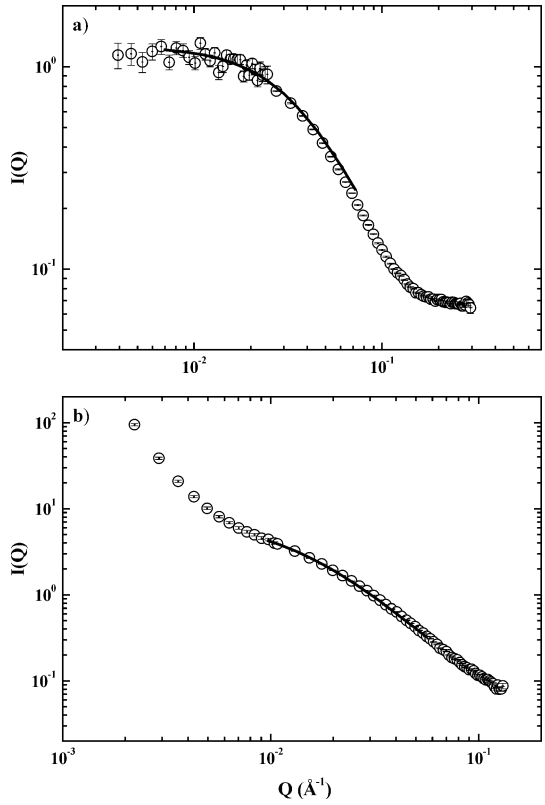

Fig. 6. SANS fits using Lorentzian line shapes. (a) AH Soluble asphaltenes: 1 wt%, 50% (v/v) toluene in heptane, 25 °C; $I_0 = 1.27 \pm 0.02$, $\xi = 29.9 \pm 0.3$, $R^2 = 0.9987$. (b) B6 Whole asphaltenes: 1 wt%, 60% (v/v) toluene in heptane, 25 °C; $I_0 = 6.7 \pm 0.1$, $\xi = 79 \pm 1$, $R^2 = 0.9974$. Note: Every other point displayed.

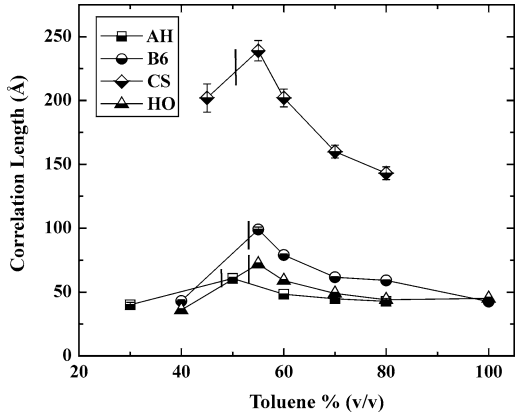

Fig. 7. Correlation lengths of Whole asphaltenes in heptol determined by SANS: 1 wt%, 25 °C. The vertical dashed lines represent the solubility limit for a 1 wt% asphaltene solution in heptol.

of heptol decreased. The maximum in correlation length was near the solubility limit of the Whole asphaltenes. Crossing the solubility limit caused agglomeration and precipitation of the largest aggregates. The resulting correlation length in the precipitated regime is only a measure of the material remaining in solution and is hence lower than the correlation lengths of the asphaltenes at the solubility limit. Aggregate ξ tended to plateau above 70% toluene, where additional

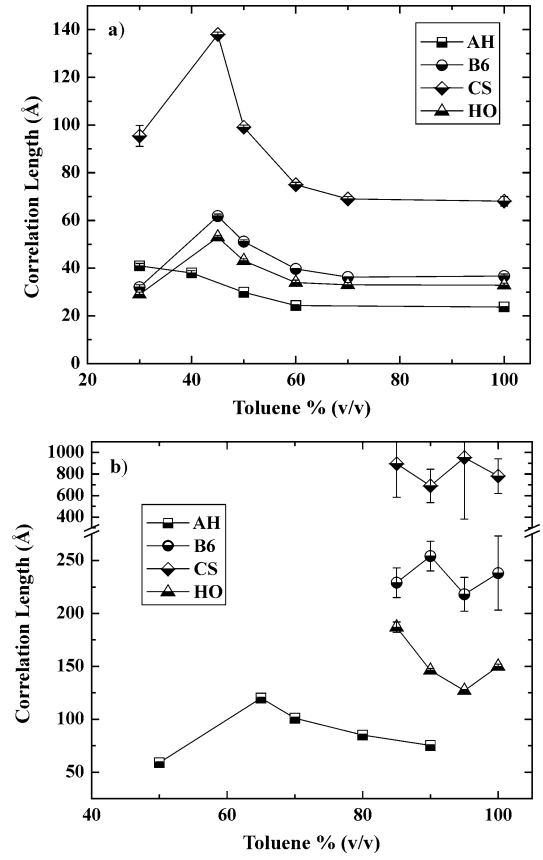

Fig. 8. Correlation lengths of (a) Soluble and (b) Precipitate asphaltenes in heptol by SANS: 1 wt%, 25 °C.

solvent aromaticity was insufficient to further disrupt interaggregate bonds. Similar behavior was seen using Cold Lake asphaltenes in mixtures of 1-methylnaphthaltene and dodecane [71]. At low to moderate asphaltene concentrations correlation lengths increased to a maximum as the aliphatic solvent volume fraction increased. Upon reaching a critical dodecane volume fraction, the correlation length decreased due to phase separation.

Differences in the solubility behavior of the Soluble and Precipitate fractions suggested that less soluble material would be more prone to aggregation. A comparison of aggregate sizes for Soluble, Whole, and Precipitate fractions (Figs. 7 and 8) indicated the Soluble fraction indeed formed the smallest aggregates while the Precipitate fraction formed the largest aggregates. Similar behavior was observed when comparing the SAXS scattering intensity curves for the Soluble and Insoluble fractions generated by Szewczyk et al. and dissolved in σ-xylene (9 wt%) [83]. The scattering intensity in the Guinier regime decreased systematically with increasing solubility. Subsequent fitting of the data to a polydisperse disk model indicated that the least soluble aggregates possessed significantly higher values for the average gyration radius, weight-average molecular weight, polydispersity, and Flory self-association constant than the more soluble fractions. Furthermore, these values were observed

to decrease with decreasing fraction aromaticity and nitrogen content.

Similar to the Whole asphaltenes, the aggregate sizes of the Soluble asphaltenes increased with decreasing solvent aromaticity, with the maximum correlation length corresponding to the limit of solubility in solution (Fig. 8a). The scattering curves for the Precipitate asphaltenes showed substantial overlap in scattering intensity between large agglomerates (Porod scattering) and smaller aggregates, and suggested a higher degree of intermolecular association than the Whole and Soluble fractions. The Precipitate fractions for B6, CS, and HO were particularly difficult to dissolve in pure toluene and, once in solution, formed large aggregates with correlation lengths ranging from ∼100 Å (HO) to ∼800 Å (CS) as shown in Fig. 8b. The CS and B6 Precipitate fractions were partially insoluble in pure toluene and aggregate size did not appear to vary with solvent conditions. As indicated in Fig. 8b, AH Precipitate remained soluble over a broad range of solution conditions with a solubility limit of ∼65% toluene that closely matched the value observed in Fig. 2a. Similarly, Fig. 2d suggested that the solubility limit of HO Precipitate was near 80% toluene and the maximum correlation length observed occurred at 85% toluene. One would expect that if additional SANS experiments were performed in which solvent aromaticity decreased below 80% toluene, the maximum correlation length for HO Precipitate asphaltenes would occur near the observed solubility limit.

An interesting observation concerning the aggregation behavior of the HO Precipitate fraction is the slight, yet reproducible, decrease in aggregate size for solutions in 95% toluene compared to pure toluene. The correlation length increased upon further heptane addition as the flocculation threshold was approached. Similar behavior was observed by Fenistein et al. for two chemically different asphaltenes dissolved in toluene with a small amount of heptane (<15 vol%) added as a flocculant [13]. The reduction in aggregate size was attributed to a decrease in the intrinsic viscosity of the solution, indicating a contraction of the aggregates. The intrinsic viscosity of the solutions tended to increase at heptane concentrations above 15 vol% and a corresponding increase in aggregate size was observed.

A comparison of scattering intensity curves for HO Whole asphaltenes in toluene and the weight-averaged summation of scattering intensities from HO Soluble and Precipitate fractions in toluene provided additional evidence that the Soluble fraction interacted with the Precipitate fraction to disrupt intraaggregate forces (Fig. 9). The total asphaltene concentration in each solution was 1 wt%. The summation intensity, I_{sum}, was weight-averaged to model the fractionation conditions according to the equation

$$I_{\text{sum}} = 0.33I_{\text{ppt}} + 0.67I_{\text{sol}}, \tag{4}$$

where I_{ppt} and I_{sol} are the scattering intensities of the Precipitate and Soluble fractions, respectively. As shown in the figure, the good agreement of the incoherent scattering intensities ($Q > 0.2$ Å^{-1}) for the Whole and summation curves,

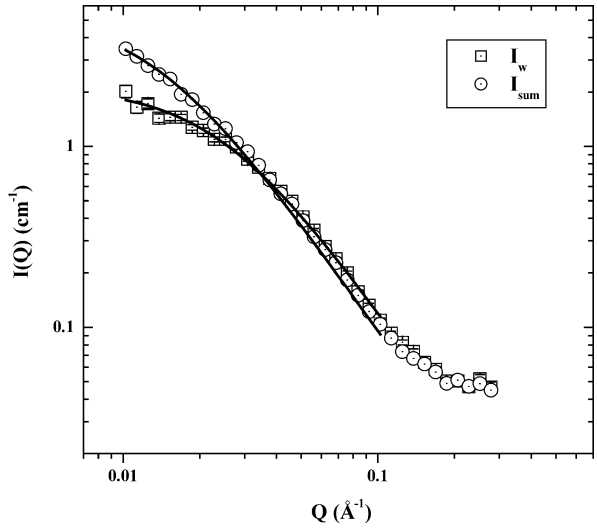

Fig. 9. Comparison of scattering intensities for HO Whole asphaltenes in toluene (I_w) and the weight-averaged summation of scattering intensities from HO Soluble and Precipitate fractions in toluene (I_{sum}). Fits of the scattering curves to Lorentzian lineshapes appear as solid lines with parameters for I_w given as I_0: 2.12 ± 0.05, ξ: 41 ± 2, R^2: 0.9573 and parameters for I_{sum} given as I_0: 5.4 ± 0.1, ξ: 74 ± 2, R^2: 0.9964. Note: Every other point displayed.

suggested that this weight averaging of the Precipitate and Soluble scattering curves was probably appropriate. Fits of the scattering curves to Lorentzian lineshapes provided correlation lengths for HO Whole and for the hypothetical recombined Whole asphaltenes of 41 Å and 74 Å, respectively. The observation that the Whole fraction had a lower correlation length than predicted by the hypothetical recombination of the fractions suggested that the Soluble fraction was indeed disrupting polar and H-bonding interactions that influenced self-association of the Precipitate fraction.

4.3. Small angle neutron scattering: 80 °C

Comparing the scattering curves and correlation lengths of the asphaltenes at 25 and 80 °C revealed dramatic but predictable temperature effects. A series of comparative scattering plots for B6 Soluble, Whole, and Precipitate at low and high temperatures is shown in Figs. 10a–10c. B6 Soluble did not show intense low-Q scattering at 25 °C and the effect of heating was minimal; correlation lengths were reduced modestly from 51 Å to 39 Å. B6 Whole and Precipitate fractions displayed a significant low-Q upturn at 25 °C that decreased in intensity with heating to 80 °C. In these two cases, scattering intensities in the range $Q < 0.01$ Å^{-1} were reduced significantly and correlation lengths decreased from 79 Å (Whole) and 240 Å (Precipitate) to 57 Å and 69 Å, respectively. The dramatic reduction of the low-Q upturn indicated that heating was effective at disrupting the largest flocs.

Table 6 presents correlation lengths of asphaltene fractions at similar heptol ratios at 25 and at 80 °C. In general, heating the samples reduced the aggregate sizes of the fractions while maintaining the same relative ordering of ag-

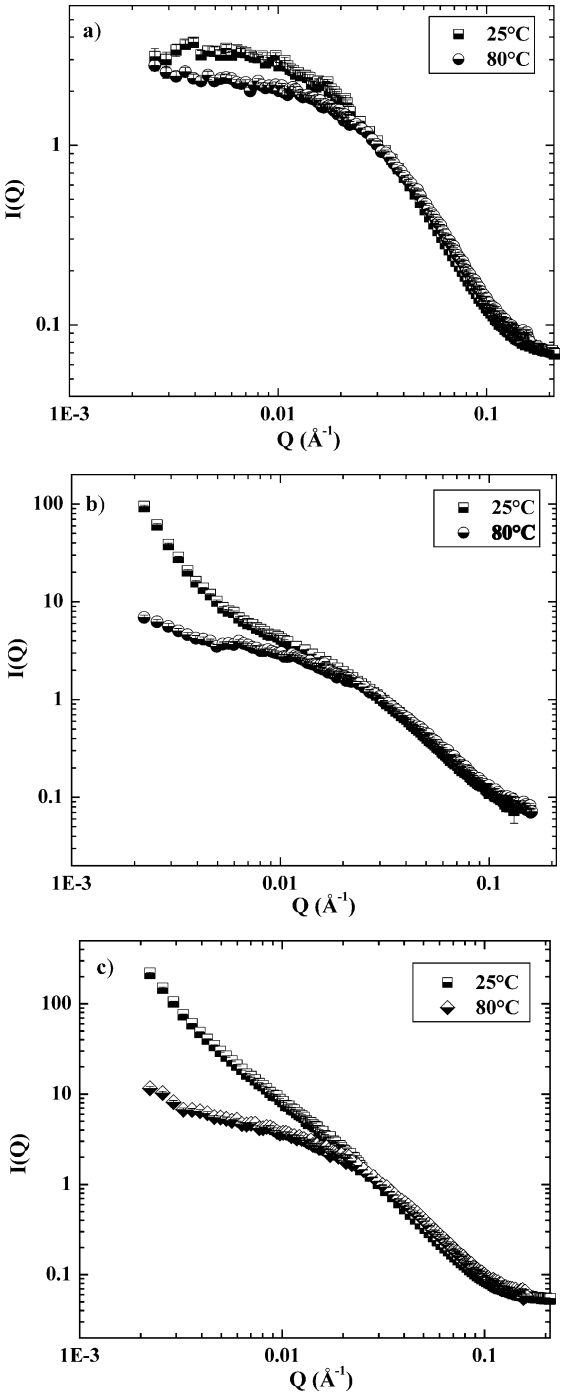

Fig. 10. SANS curves of asphaltenes (1 wt%) in heptol: (a) B6 Soluble in 50% toluene; (b) B6 Whole in 60% toluene; (c) B6 Precipitate in 100% toluene.

gregate sizes between fractions and crude sources that was observed at 25 °C (i.e., $\xi_{\text{Soluble}} < \xi_{\text{Whole}} < \xi_{\text{Precipitate}}$ and $\xi_{\text{AH}} < \xi_{\text{HO}} < \xi_{\text{B6}} < \xi_{\text{CS}}$). In addition, reduction of low-Q upturn extended the Guinier plateau to a lower Q range and reduced the uncertainty in aggregate sizes. The Precipitate fraction was generally the most responsive to heating, with greater than twofold reductions in aggregate size. The relative reductions in the low-Q scattering intensities with

Table 6
Correlation length (Å) of Whole, Soluble, and Precipitate asphaltenes in heptol at 25 and 80 °C: 1 wt%

Asphaltene fraction			ξ (Å)	
Asph.	Fraction	% toluene	25 °C	80 °C
AH	Soluble	40	38 ± 1	30 ± 1
AH	Whole	50	61 ± 1	36 ± 1
B6	Soluble	50	51 ± 1	39 ± 1
B6	Whole	55	99 ± 2	65 ± 1
B6	Whole	60	79 ± 1	57 ± 1
B6	Whole	80	59 ± 1	44 ± 1
B6	Precipitate	85	230 ± 10	89 ± 1
B6	Precipitate	90	250 ± 10	82 ± 1
B6	Precipitate	100	240 ± 40	69 ± 1
CS	Soluble	60	75 ± 1	51 ± 1
CS	Soluble	100	68 ± 2	42 ± 1
CS	Whole	60	202 ± 7	74 ± 1
CS	Whole	80	143 ± 5	57 ± 1
CS	Precipitate	90	700 ± 200	104 ± 2
HO	Soluble	50	43 ± 1	39 ± 1
HO	Whole	100	45 ± 1	32 ± 1
HO	Precipitate	90	146 ± 2	62 ± 1
HO	Precipitate	100	150 ± 2	55 ± 1

increasing temperature for the various fractions suggested a high degree of intraaggregate bonding in the Precipitate fractions. The process of fractionation typically enriched the least soluble asphaltenes with polar and aromatic moieties, species that were likely responsible for aggregation and flocculation.

The relative polarity and aromaticity of B6 asphaltenic fractions compared to CS asphaltenic fractions also appeared to affect the responses of the aggregates to heating. On a percentage change in correlation length basis, CS Precipitate aggregates that are primarily stabilized through π-bonding interactions showed a larger decrease in ξ with heating than B6 Precipitate aggregates, which are mainly stabilized through polar and hydrogen-bonding interactions. The disruption of dispersion and π–π bonding interactions in CS Precipitate at 53 °C might explain the similarities between the molar masses of CS Precipitate and CS Whole determined from VPO. Similarly, heating of B6 Precipitate to 53 °C was apparently not effective at disrupting the stronger polar and hydrogen-bonding forces that dominated self-aggregation in this fraction. Hence, significant differences were observed between the molar masses of the B6 Whole and Precipitate fractions.

An attempt was made to find the aggregate size corresponding to an asphaltene monomer or irreducible oligomer by dissolving each of the asphaltene fractions in deuterated 1-methylnaphthalene. This solvent was more aromatic with a larger molecular dimension than toluene, suggesting that it may interact more effectively with asphaltene aggregates through dispersion forces. A comparison of correlation lengths obtained for the various asphaltene fractions in toluene and 1-methylnaphthalene at 80 °C is shown in Table 7. In all cases, 1-methylnaphthalene was a better solvent for asphaltenes than toluene, with the largest reduction in

Table 7
Correlation length (Å) of asphaltenes in 1-methylnaphthalene and toluene (80 °C)

Asphaltene	Soluble		Whole		Precipitate	
	MN	Tol	MN	Tol	MN	Tol
AH	18.5 ± 0.2		23.9 ± 0.2	28.1 ± 0.6	30.2 ± 0.3	39.2 ± 0.6
B6	23.7 ± 0.5	28.1 ± 0.6	35.6 ± 0.8	40.0 ± 0.7	51.0 ± 0.8	69 ± 1
CS	33.8 ± 0.8	41.7 ± 0.7	39.6 ± 0.8	48 ± 1	47.0 ± 0.8	80 ± 2
HO	23.0 ± 0.2		29.5 ± 0.6	31.5 ± 0.7	45.4 ± 0.9	55 ± 1

aggregate sizes occurring in the Precipitate fractions. As expected, CS Precipitate, with its aggregation behavior dominated by dispersion forces and π–π bonding interactions, showed the largest reduction in aggregate size (∼41%). Most other fractions showed a reduction in correlation length of 10–25% when dissolved in 1-methylnaphthalene instead of toluene. It would be difficult to further reduce aggregate sizes except by dissolution in a more polar solvent (e.g., a 1-methylnaphthalene/methanol mixture) or by addition of a solvating agent (such as resins).

In all cases, Soluble asphaltenes were affected the least and Precipitate asphaltenes were affected the most by the temperature increase. This evidence suggests the Precipitate fraction was enriched with temperature-sensitive intermolecular bonds—most likely hydrogen bonds. Another possibility for the occurrence and disappearance of low-Q scattering features with temperature fluctuations that must be discarded is the that waxes were co-precipitated with the asphaltenes during their preparation and subsequent fractionation. Most waxes have melting points above 60–70 °C, which could explain the disappearance of a low-Q upturn at 80 °C; however, Bragg scattering peaks that are indicative of crystallinity were not evident in the scattering curves at 25 °C. To rule out the possibility of wax contamination, high temperature simulated distillation (HTSimDist) was performed on B6 and CS Whole [85]. Neither B6 nor CS asphaltenes contained any discernable wax peaks. These findings ruled out the possibility of neutron scattering from non-asphaltenic structures that may be present in crude oil. Each of the aggregation phenomena seen resulted from the propensity of asphaltenes to form aggregates mediated by intermolecular bonding.

5. Conclusions

The solubility behaviors, chemical properties, and aggregation extents of four asphaltenes and their soluble and insoluble fractions were examined. Whole, unfractionated asphaltenes were soluble to filtration in heptol containing greater than 52% (v/v) toluene. The more and less soluble fractions had solubility limits approximately 10% (v/v) lower and 30% (v/v) higher in toluene, respectively, than the corresponding Whole asphaltenes. The mechanism of precipitation was controlled by dispersion interactions between the asphaltenes and solvent; however, the tendency of the less soluble fractions to precipitate in toluene suggested that the Soluble fraction served to disrupt the strong polar and hydrogen-bonding interactions that drive self-association in the Precipitate fraction. Further evidence of a cooperative interaction between the Soluble and Precipitate fractions was observed from the SANS studies. The observation that HO Whole asphaltenes had a lower correlation length than predicted by the hypothetical recombination of the Soluble and Precipitate fractions suggested cooperative interaction of the more and less soluble fractions.

In general, several key trends were demonstrated by the neutron scattering behavior of asphaltene–heptol systems. For example, aggregate correlation length increased with decreasing solvent aromaticity up to the solubility limit, beyond which the aggregate size decreased with heptane addition. The maximum in soluble aggregate size, as calculated from the Lorentzian portion of the scattering curve in the accessible Q range, always appeared at the limit of asphaltene solubility. Crossing the solubility limit caused significant agglomeration and precipitation of the largest aggregates that, consequently, consisted of the most polar and aromatic asphaltenes. After precipitation, the remaining soluble material tended to form smaller, more labile aggregates with dispersion forces as the dominant contribution to aggregation behavior.

Number average molar masses determined by VPO in toluene at 53 °C indicated that B6 Precipitate asphaltenes were more highly aggregated than the corresponding B6 Whole and Soluble fractions. The CS Precipitate and Whole fractions had similar molar mass values that were slightly higher than those observed for B6 Whole asphaltenes. The relatively low molar mass of the CS Precipitate fraction relative to the B6 Precipitate fraction suggested a distinct difference in the aggregation mechanisms of the two fractions.

By comparing the elemental analysis, VPO, and SANS results, we can deduce the mechanisms that influence the solubility and aggregation of asphaltenes in solution. Of the four crude asphaltenes, CS asphaltenes formed the largest aggregates in heptol. The solubility mechanism for CS asphaltenes appeared to be dominated by aromatic π–π bonding interactions due to their relatively low H/C ratio (∼1.1) and nitrogen content (∼1.3% w/w). B6 and HO asphaltenes formed similar-sized aggregates in heptol that were smaller than the corresponding CS subfractions. With B6 and HO asphaltenes, the solubility mechanism was likely driven by polar interactions due to their high H/C ratios (>1.2) and relatively high nitrogen contents (1.8 to 2.1% w/w). AH asphaltenes, possessing the lowest nitrogen contents (0.9 to

1.1% w/w) and relatively low H/C ratios, formed the smallest aggregates in heptol. The ability to participate in polar and H-bonding interactions was the major difference in the aggregation behaviors of CS and AH asphaltenes, the largest and smallest aggregate formers, respectively.

The presence of a Porod feature in the neutron scattering curves indicated the asphaltene solutions contained both individual aggregates and a portion of highly aggregated or precipitated material larger than 1000 Å in size. Heating the samples to 80 °C aided the dissolution of the agglomerates and was effective at reducing the intensity of the low-Q scattering. The observation that heating was most effective at reducing the correlation lengths of the less soluble asphaltenes suggested that temperature-sensitive interaggregate bonds, most likely hydrogen bonds, were being broken. Similarities in correlation length between samples prepared at 25 °C and samples that were heated to 80 °C and then allowed to cool back to 25 °C suggested that heating the samples to aid dissolution did not appear to adversely affect the scattering measurements. Aggregate sizes were further reduced when measurements were performed in 1-methylnaphthalene (a more dispersive solvent) rather than toluene. Methylnaphthalene was most effective at reducing the aggregate sizes of CS Precipitate asphaltenes, an observation consistent with the notion that aggregation in CS asphaltenes is dominated by dispersion and π–π bonding forces rather than polar interactions. It was suggested that aggregate sizes could be further reduced by dissolution in a more polar solvent, such as a mixture of 1-methylnaphthalene/methanol, or by the addition of solvating resins.

Fractionation appears to concentrate the more polar species into the least soluble subfraction as indicated by elemental analysis. SANS data indicate that the less soluble (more polar) asphaltenes contribute the majority of the species responsible for asphaltene aggregation in solution. This more polar, less soluble fraction is likely the major cause for many petroleum production problems such as pipeline deposition and water-in-oil emulsion stabilization.

Acknowledgments

This research has been supported by PERF 97-07, Industrial Emulsion Consortium, ExxonMobil, Shell, Chevron-Texaco, Ondeo-Nalco, and the National Science Foundation (CTS9817127). We thank Eric Sirota of ExxonMobil Corporate Research and Min Lin of NIST for their assistance on the NG-7 and NG-1 beamlines. We acknowledge the support of the National Institute of Standards and Technology, U.S. Department of Commerce, in providing the neutron research facilities used in this work. This work utilized facilities supported in part by the National Science Foundation under Agreement DMR-9986442. This work benefited from the use of facilities in the Intense Pulsed Neutron Source and the Chemistry Division, which is funded by the U.S. Department of Energy, Office of Basic Energy Sciences under contract W-31-109-ENG-38 to the University of Chicago. We particularly thank to Pappannan Thiyagarajan and Denis Wozniak for their assistance on the SAND instrument. We also thank Marit-Helen Ese, Jihong Tong, and George Blankenship for helping with the sample preparation and SANS data collection. We are grateful to Paul Lindemuth of Ondeo Nalco Energy Services for facilitating the ICP metals analyses and Darlene Mahlow at the University of Alberta for performing the elemental analyses (C, H, N, S, O) and vapor pressure osmometry experiments.

References

[1] F.J. Nellensteyn, J. I. Petrol. Technol. 10 (1924) 311.
[2] J.P. Pfeiffer, R.N.J. Saal, J. Phys. Chem. 44 (1940) 139.
[3] H. Neumann, Petrochemie 18 (1965) 776.
[4] J.P. Dickie, T.F. Yen, Anal. Chem. 39 (14) (1967) 1847.
[5] S.A. Berridge, M.T. Thew, A.G. Loriston-Clarke, J. I. Petrol. 54 (539) (1968) 333.
[6] J.G. Speight, Fuel 50 (1971) 102.
[7] J.G. Speight, S.E. Moschopedis, Prepr. ACS Div. Pet. Chem. 24 (4) (1979) 910.
[8] J.C. Ravey, G. Ducouret, D. Espinat, Fuel 67 (11) (1988) 1560.
[9] E.Y. Sheu, M.M.D. Tar, D.A. Storm, Macromol. Rep. A 28 (1991) 159.
[10] B. Siffert, C. Bourgeois, E. Papirer, Fuel 63 (6) (1984) 834.
[11] P. Herzog, D. Tchoubar, D. Espinat, Fuel 67 (1988) 245.
[12] C. Bardon, L. Barre, D. Espinat, V. Guille, M.H. Li, J. Lambard, J.C. Ravey, E. Rosenberg, T. Zemb, Fuel Sci. Technol. Int. 14 (1–2) (1996) 203.
[13] D. Fenistein, L. Barre, D. Broseta, D. Espinat, A. Livet, J.N. Roux, M. Scarsella, Langmuir 14 (5) (1998) 1013.
[14] G.W. Mushrush, J.G. Speight, Petroleum Products: Instability and Incompatibility, Taylor & Francis, Bristol, PA, 1995.
[15] D.A. Storm, S.J. DeCanio, E.Y. Sheu, in: T.F. Yen (Ed.), Asphaltene Particles in Fossil Fuel Exploration, Recovery, Refining, and Production Processes, Plenum, New York, 1994, p. 81.
[16] J.-R. Lin, J.-K. Park, T.F. Yen, in: T.F. Yen (Ed.), Asphaltene Particles in Fossil Fuel Exploration, Recovery, Refining, and Production Processes, Plenum, New York, 1994, p. 91.
[17] R. Cimino, S. Correra, A.D. Bianco, T.P. Lockhart, in: O.C. Mullins (Ed.), Asphaltenes: Fundamentals and Applications, Plenum, New York, 1995, p. 97.
[18] H. Fordedal, Y. Schildberg, J. Sjoblom, J.-L. Volle, Colloids Surf. A 106 (1996) 33.
[19] J.E. Strassner, J. Pet. Technol. 20 (1968) 303.
[20] J. Sjöblom, O. Urdahl, K.G.N. Borve, L. Mingyuan, J.O. Saeten, A.A. Christy, T. Gu, Adv. Colloid Interface Sci. 41 (1992) 241.
[21] S.E. Taylor, Chem. Ind. 20 (1992) 770.
[22] M. van der Waarden, Kolloid Z. Z. Polym. 156 (2) (1958) 116.
[23] H.J. Neumann, B. Paczynska-Lahme, Chem. Eng. Technol. 53 (1981) 911.
[24] E.Y. Sheu, M.B. Shields, in: SPE International Symposium on Oilfield Chemistry, SPE 28995, 1995, p. 523.
[25] J.D. McLean, P.K. Kilpatrick, J. Colloid Interface Sci. 189 (1997) 242.
[26] J.D. McLean, P.M. Spiecker, A.P. Sullivan, P.K. Kilpatrick, in: E.Y. Sheu (Ed.), Structures and Dynamics of Asphaltenes, Plenum, New York, 1998, p. 377.
[27] D.L. Mitchell, J.G. Speight, Fuel 52 (4) (1973) 149.
[28] T.F. Yen, J.G. Erdman, S.S. Pollack, Anal. Chem. 33 (11) (1961) 1587.
[29] M.M. Boduszynski, Energy Fuels 2 (5) (1988) 597.
[30] M.A. Bestougeff, P. Gendrel, Prepr. ACS Div. Pet. Chem. 9 (2) (1964) B51.

[31] J.F. McKay, D.R. Latham, W.E. Haines, Fuel 60 (1) (1981) 27.
[32] M.M. Boduszynski, Prepr. ACS Div. Pet. Chem. 30 (1985) 626.
[33] J.G. Speight, Fuel 49 (1970) 76.
[34] W.R. Biggs, R.J. Brown, J.C. Fetzer, Energy Fuels 1 (3) (1987) 257.
[35] V. Nalwaya, V. Tangtayakom, P. Piumsomboon, S. Fogler, Ind. Eng. Chem. Res. 38 (3) (1999) 964.
[36] J.G. Reynolds, W.R. Biggs, Fuel Sci. Technol. Int. 4 (6) (1986) 749.
[37] J.G. Reynolds, W.R. Biggs, Accounts Chem. Res. 21 (9) (1988) 319.
[38] J.G. Reynolds, E.L. Jones, J.A. Bennett, W.R. Biggs, Prepr. ACS Div. Pet. Chem. 33 (2) (1988) 239.
[39] H.H. Hasiba, F.W. Jessen, J. Can. Pet. Technol. 7 (1) (1968) 1.
[40] J.C. Petersen, Anal. Chem. 47 (1) (1975) 112.
[41] S.I. Andersen, Fuel Sci. Technol. Int. 12 (1) (1994) 51.
[42] C.L. Chang, H.S. Fogler, Langmuir 10 (6) (1994) 1749.
[43] M.U. Hasan, M.N. Siddiqui, M. Arab, Fuel 67 (8) (1988) 1131.
[44] J.M. Jacobson, M.R. Gray, Fuel 66 (6) (1987) 749.
[45] R.V. Barbour, J.C. Petersen, Anal. Chem. 46 (2) (1974) 273.
[46] M.M. Boduszynski, J.F. McKay, D.R. Latham, Proc. Assoc. Asphalt Pav. Technol. 49 (1980) 123.
[47] T. Ignasiak, O.P. Strausz, D.S. Montgomery, Fuel 56 (1977) 359.
[48] S.E. Moschopedis, J.G. Speight, Fuel 55 (1976) 187.
[49] J.C. Petersen, Fuel 46 (4–5) (1967) 295.
[50] H.P. Maruska, M.L. Rao, Fuel Sci. Technol. Int. 5 (2) (1987) 119.
[51] R.E. Overfield, E.Y. Sheu, S.K. Sinha, K.S. Liang, Fuel Sci. Technol. Int. 7 (5–6) (1989) 611.
[52] E.Y. Sheu, D.A. Storm, M.M.D. Tar, J. Non-Cryst. Solids 131–133 (1991) 341.
[53] M.M.H. Al-Jarrah, A.H. Al-Dujaili, Fuel Sci. Technol. Int. 7 (1) (1989) 69.
[54] S. Acevedo, B. Mendez, A. Rojas, I. Layrisse, H. Rivas, Fuel 64 (1985) 1741.
[55] I.A. Wiehe, K.S. Liang, Fluid Phase Equilibr. 117 (1–2) (1996) 201.
[56] J.F. McKay, P.J. Amend, T.E. Cogswell, P.M. Harnsberger, R.B. Erickson, D.R. Latham, in: S. Siggia (Ed.), Analytical Chemistry of Liquid Fuel Sources: Tar Sands, Oil Shale, Coal, and Petroleum, in: ACS Advances in Chemistry Series, Vol. 170, American Chemical Society, Washington, DC, 1978, p. 128.
[57] S.I. Andersen, A. Keul, E. Stenby, Pet. Sci. Technol. 15 (7–8) (1997) 611.
[58] H.W. Yarranton, J.H. Masliyah, AIChE J. 42 (12) (1996) 3533.
[59] H.W. Yarranton, H. Alboudwarej, R. Jakher, Ind. Eng. Chem. Res. 39 (8) (2000) 2916.
[60] J.C. Ravey, D. Espinat, Prog. Colloid Polym. Sci. 81 (1990) 127.
[61] E.Y. Sheu, M.M.D. Tar, D.A. Storm, Prepr. ACS Div. Fuel Chem. 37 (2) (1992) 844.
[62] D. Espinat, J.C. Ravey, V. Guille, J. Lambard, T. Zemb, J.P. Cotton, J. Phys. IV 3 (C8) (1993) 181.
[63] D.A. Storm, E.Y. Sheu, M.M. Detar, Fuel 72 (7) (1993) 977.
[64] P. Thiyagarajan, J.E. Hunt, R.E. Winans, K.B. Anderson, J.T. Miller, Energy Fuels 9 (5) (1995) 829.
[65] Y.N. Xu, Y. Koga, O.P. Strausz, Fuel 74 (7) (1995) 960.
[66] Y.C. Liu, E.Y. Sheu, S.H. Chen, D.A. Storm, Fuel 74 (9) (1995) 1352.
[67] H. Rassamdana, M. Sahimi, AIChE J. 42 (12) (1996) 3318.
[68] L. Barre, D. Espinat, E. Rosenberg, M. Scarsella, Rev. Inst. Fr. Pet. 52 (2) (1997) 161.
[69] M.Y. Lin, E.B. Sirota, H. Gang, Abstr. Pap. Am. Chem. Soc. 213 (1997) 66.
[70] J.T. Miller, R.B. Fisher, P. Thiyagarajan, R.E. Winans, J.E. Hunt, Energy Fuels 12 (6) (1998) 1290.
[71] E.B. Sirota, Pet. Sci. Technol. 16 (3–4) (1998) 415.
[72] D. Fenistein, L. Barre, Fuel 80 (2) (2001) 283.
[73] T.G. Savvidis, D. Fenistein, L. Barre, E. Behar, AIChE J. 47 (1) (2001) 206.
[74] J.N. Roux, D. Broseta, B. Deme, Langmuir 17 (16) (2001) 5085.
[75] E.Y. Sheu, K.S. Liang, S.K. Sinha, R.E. Overfield, J. Colloid Interface Sci. 153 (2) (1992) 399.
[76] G. Porte, H.G. Zhou, V. Lazzeri, Langmuir 19 (1) (2003) 40.
[77] T.J. Kaminski, H.S. Fogler, N. Wolf, P. Wattana, A. Mairal, Energy Fuels 14 (1) (2000) 25.
[78] P.-G. de Gennes, Scaling Concepts in Polymer Physics, Cornell Univ. Press, Ithaca, NY, 1979.
[79] C.M. Hansen, Ind. Eng. Chem. Prod. Res. Dev. 8 (1) (1969) 2.
[80] A.F.M. Barton, CRC Handbook of Solubility Parameters and Other Cohesion Parameters, CRC Press, Boca Raton, FL, 1983.
[81] J.S. Buckley, Fuel Sci. Technol. Int. 14 (1–2) (1996) 55.
[82] J.S. Buckley, Energy Fuels 13 (2) (1999) 328.
[83] V. Szewczyk, F. Behar, E. Behar, M. Scarsella, Rev. Inst. Fr. Pet. 51 (4) (1996) 575.
[84] M.F. Ali, H. Perzanowski, A. Bukhari, A.A. Al-Haji, Energy Fuels 7 (2) (1993) 179.
[85] P.M. Spiecker, Ph.D. thesis, North Carolina State University, 2001.